Adaptive Observer-based parameter estimation with application to Road Gradient and Vehicle Mass Estimation

Muhammad Nasiruddin Mahyuddin, *Member, IEEE,* Jing Na, Guido Herrmann, *Senior Member, IEEE,* Xuemei Ren and Phil Barber

***Abstract*—A novel observer-based parameter estimation scheme with sliding mode term has been developed to estimate the road gradient and the vehicle weight using only the vehicle's velocity and the driving torque. The estimation algorithm exploits all known terms in the system dynamics and a low pass filtered representation of the dynamics to derive an explicit expression of the parameter estimation error without measuring the acceleration. The proposed parameter estimation scheme which features a sliding-mode term to ensure the fast and robust convergence of the estimation in the presence of persistent excitation is augmented to an adaptive observer and analyzed using Lyapunov Theory. The analytical results show that the algorithm is stable and ensures finite-time error convergence to a bounded error even in the presence of disturbances. In the absence of disturbances, convergence to the true values in finite time is guaranteed. A simple practical method for validating persistent excitation is provided using the new theoretical approach to estimation. This is validated by the practical implementation of the algorithm on a small-scaled vehicle, emulating a car system. The slope gradient as well as the vehicle's mass/weight are estimated online. The algorithm shows a significant improvement over previous results.**

I. INTRODUCTION

In recent years, improving safety of the drivers and protecting the environment from excessive carbon emission and fuel consumption have become the main agenda of automotive companies. Several results in the literature evidently show the motivation of harnessing the knowledge of road gradient and vehicle's mass [1]-[7], for the purpose of delivering safety features and fuel efficiency in vehicular technology. Active safety technologies such as vehicle stability control [8],[9] and antilock braking systems [10],[11] promise better control of the vehicle in the midst of aggressive maneuvers, minimising the likelihoods of rollover and skidding. UK research indicates the effectiveness of reducing serious crashes involving loss of control situations such as skidding, and rollover as much as 33% and 59% respectively [12]. These active safety technologies require information on the vehicle's inertial parameter such as mass in order to perform prior system calibration. To add further challenge, trucks and SUVs are vehicles with highly variable loads. Nominal loads may provide high load safety but at the expense of the need of load calibration in case of load changes [13], [2]. Adapting active safety systems to variations in loading is the solution to the calibration problem, in particular, the online estimation of mass of the vehicle across all varying loads.

It has been shown that mass estimation without the knowledge of road grade proves to be ineffective as the method would contain an unacceptable level of error [1]. Knowledge of the road grade can be used in engine and gearbox control systems to assist the instantaneous power demand whilst regulating fuel consumption and thus, keeping environmental impact as low as possible [14]. Acceleration performance of a vehicle on a steep downhill can be improved in terms of hill holding, traction control and transmission shift scheduling, simultaneously giving the vehicle the merits of safety and fuel efficiency [6]. The reasons above prompt us to obtain the road gradient and vehicle's mass simultaneously in a reliable and economic way.

Sensor-based methods to obtain road gradient information are prevalent [14], [15], [16]. Extraneous hardware and wiring complexity as consequence of additional sensors may not be desirable for automotive manufacturers [5]. One may argue that the cost of an accelerometer-based sensor, such as an inclinometer may be acceptable. However, due to the nature of the inclinometer's construction, it is so susceptible to giving out errors [17] as it is only suited to measure static inclination. Exploiting remote sensing methods such as GPS, e.g. in [14], may aid in road gradient estimation but at some cost. In [2], a GPS or barometer sensor is utilized in addition to torque and velocity sensors to obtain absolute road height information, while Barrho, et al. [18] require accurate information of the vehicle mass which is not always possible.

There is some work adopting a sensorless or model-based approach in road gradient and vehicle's mass estimation [13],[1],[7],[19],[5],[4]. Mangan et al. [5] adopt a sensorless longitudinal road gradient estimation method which proves

Manuscript received September 1, 2012; revised December 23, 2012 and April, 9 2013. Accepted for publication June 10, 2013.

*Muhammad Nasiruddin Mahyuddin is currently a PhD student in the Department of Mechanical Engineering, University of Bristol, BS8 1TR, UK. and a staff on study-leave of Universiti Sains Malaysia. Email: memnm@bristol.ac.uk or nasiruddin@ieee.org

**Jing Na is with the Faculty of Mechanical and Electrical Engineering, Kunming University of Science and Technology, Kunming 650093, China, (e-mail: najing25@163.com)

***Guido Herrmann is a Reader in Control and Dynamics at the Department of Mechanical Engineering, University of Bristol. BS8 1TR, UK. Email:g.herrmann@bristol.ac.uk

****Xuemei Ren is a Professor at School of Automation, Beijing Institute of Technology, Beijing, 100081,China, E-mail:xmren@bit.edu.cn

*****Phil Barber is with Jaguar and Land Rover Research, W/2/021 Engineering Centre, Abbey Road, Whitley, Coventry CV 4LF, UK.

to be effective, although reliance on acceleration information, through differentiated velocity, may expose estimation to be over-sensitive to noise. Bae et al. [1] suggest a recursive least-squares (RLS) approach which requires acceleration information and then assumes the existence of sufficient data points to solve for the missing parameters, i.e. vehicle mass and gradient, by inverting a regressor matrix in a batch process. Similarly, the work in [20] and [6] estimate the road grade only using the position, velocity and driving torque or force signal. In [7], an RLS-based observer is designed to estimate the road gradient only, with the knowledge of the vehicle's mass.

In this paper, we revisit the online road gradient and mass estimation of vehicular systems using only the vehicle's velocity and the driving torque. This is achieved based on a novel adaptive nonlinear observer design. A novel estimation algorithm guarantees finite-time convergence of the estimated parameters to the true values. Moreover, auxiliary filtered variables implicitly generate a parameter estimation error which drives the adaptation algorithm with finite-time convergence. Compared to previous results (e.g. [21]) concerning the parameter estimation, some appropriate information of the parameter error is derived, and then incorporated into the parameter adaptation for the observer design. The proposed method is verified experimentally in a reduced-scale vehicular system, which provides a significant improvement over a previous algorithm. Moreover, the adaptation scheme does not rely on acceleration information due to some auxiliary filters. In addition, the parameter estimation scheme uses a filtered regressor matrix. Measurable system states, a regressor vector and the known dynamics are collected and filtered to form auxiliary variables. Owed to the special feature of a sliding mode term, the adaptation algorithm guarantees robust finite-time convergence to a compact set, provided that there is a Persistent Excitation (PE) condition fulfilled so that a filtered regressor matrix remains positive definite. The parameter error information can be explicitly formulated by virtue of the filtered auxiliary variables. The possible instability and infinite growth found in [22] and [23] due to the existence of an unstable integrator are prevented in this paper. We also show robustness of our adaptive scheme and *we can verify* the PE condition through computation of the respective filtered regressor matrix's condition number. In contrast, the classical RLS algorithm fundamentally lacks in fast convergence, specifically exponential convergence, let alone finite-time convergence [21],[24].

Based on the discussions above, the contributions made in the paper can be summarised as follows:

- The proposed estimation approach does not require the knowledge of vehicle's acceleration, i.e. only velocity and torque is needed.
- The adaptive observer-based parameter estimation algorithm proposed here incorporates a novel adaptive law that captures the parameter estimation error.
- Finite-time convergence of parameter estimate to true values is guaranteed in the presence of PE or sufficient richness (SR), in the absence of unknown disturbances. This is simultaneously achievable with being robust.
- The adaptive law incorporated in the proposed algorithm scheme contains significant robustness against disturbances. The sliding-mode term allows the switching signal to effectively reject disturbances and uncertainties.
- Extensive comparative experimental analysis provide evidence of the advantages of our approach in comparison to the RLS-algorithm.

This paper is organised as follows: In Section II, a system formulation is presented in a generic form along with the required assumption. Section III presents the adaptive observer design together with the novel adaptive law design in Section IV. A stability analysis is discussed in Section V followed by Section VI which presents the main contribution of the paper; the parameter estimation algorithm in application to road gradient and vehicle's weight estimation. Section VII describes the experimental process and the main results of the contribution. Section VIII concludes the paper.

II. System Formulations

Consider a nonlinear system of the following structure:

$$\begin{aligned} \dot{x} &= Ax + B_1 u_1 + B_2 f(x, u_2) + \zeta \\ y &= Cx \end{aligned} \tag{1}$$

where $A \in \mathbb{R}^{n\times n}$ is the known system matrix, $B_1 \in \mathbb{R}^{n\times m_1}$ and $B_2 \in \mathbb{R}^{n\times m_2}$ are known input matrices, $u_1 \in \mathbb{R}^{m_1}$ and $u_2 \in \mathbb{R}^{\bar{m}_2}$ are known inputs, whilst $C \in \mathbb{R}^{p\times n}$ is the corresponding output matrix and $\zeta \in L_\infty$ is a bounded disturbance. The function $f(x, u_2) : \mathbb{R}^n \times \mathbb{R}^{\bar{m}_2} \to \mathbb{R}^{m_2}$ is partially unknown for which the detail will be outlined below and the pair (A, B_1) is controllable. It is assumed that $p \geq m_2$. The following assumptions are made:

Assumption 1 (C, A, B_2) is minimum phase and (CB_2) is full rank.

Assumption 2 The function $f(x, u_2)$ can be represented in a linear parameterized form: $f(x, u_2) = \varphi(x, u_2)\Theta$, where $\varphi : \mathbb{R}^n \times \mathbb{R}^{m_2} \to \mathbb{R}^{m_2\times l}$ is a known Lipschitz continuous function, while $\Theta = const., \Theta \in \mathbb{R}^l$ is an unknown parameter vector which is to be estimated.

Assumption 3 The signals x, u_1 and u_2 are measurable and bounded.

Assumption 3 is a common assumption for observer design and can be easily achieved by suitable choice of the control signal u_1 (e.g. [22] [26]).

Under these conditions, the system can take the following structure

$$\begin{aligned} \begin{bmatrix} \dot{x}_1 \\ \dot{x}_2 \end{bmatrix} &= \begin{bmatrix} A_{11} & A_{12} \\ A_{21} & A_{22} \end{bmatrix} \begin{bmatrix} x_1 \\ x_2 \end{bmatrix} + \\ &\quad \begin{bmatrix} B_{11} \\ B_{12} \end{bmatrix} u_1 + \begin{bmatrix} 0 \\ \bar{B}_2 \end{bmatrix} \varphi\Theta + \begin{bmatrix} \zeta_1 \\ \zeta_2 \end{bmatrix} \\ y &= [0 \quad I] \begin{bmatrix} x_1 \\ x_2 \end{bmatrix} \end{aligned} \tag{2}$$

where $\bar{B}_2 \in \mathbb{R}^{p\times m_2}$, $I \in \mathbb{R}^{p\times p}$ and $x_2 = Cx$. Note that this reformulation is always possible from Assumptions 1 and 3 using Proposition 6.3 in [26]. Moreover, we make the following assumption.

Assumption 4 $A_{21} = 0$, i.e. the second state equation in (2)

is decoupled.
Assumption 4 is possibly a strong assumption but it will fit the generic practical system structures (e.g. vehicular) investigated in this paper.

III. Adaptive Observer Design

We will design an adaptive observer to estimate the state vectors which will be suitably combined with a *novel* parameter estimation algorithm. The adaptive observer takes the following form:

$$\dot{\hat{x}} = A\hat{x} + B_1 u_1 + B_2\varphi\hat{\Theta} + L(y - C\hat{x}) \quad (3)$$

where $\hat{x}$ is the estimated state vector, $\hat{\Theta}$ is the estimated parameter vector. L is the observer gain matrix such that $A_c = A - LC$ is a stable matrix and there exist, according to Proposition 6.3 in [26], positive definite matrices, P and Q so that,

$$A_c^T P + PA_c = -Q \quad (4)$$

where,

$$P = \begin{bmatrix} P_1 & 0 \\ 0 & P_2 \end{bmatrix} > 0, \quad (5)$$

$$Q = \begin{bmatrix} Q_1 & Q_{12} \\ Q_{12}^T & Q_2 \end{bmatrix} > 0, \quad PB_2 = C^T F^T \quad (6)$$

and $F \in \mathbb{R}^{m_2 \times p}$ is a positive definite matrix. From (4), it follows,

$$\begin{bmatrix} A_{c11}^T P_1 + P_1 A_{c11} & P_1 A_{c12} \\ A_{c12}^T P_1 & P_2 A_{c22} + A_{c22}^T P_2 \end{bmatrix} = -Q \quad (7)$$

and $A_{c21} = 0$. Let $\tilde{x} = x - \hat{x}$ and $\tilde{\Theta} = \Theta - \hat{\Theta}$. We can then use (1) and (3) to define the error dynamics $\tilde{x} = x - \hat{x}$ as

$$\begin{aligned} \dot{\tilde{x}} &= (A - LC)\tilde{x} + B_2\varphi\tilde{\Theta} + \zeta \\ &= A_c\tilde{x} + B_2\varphi\tilde{\Theta} + \zeta \end{aligned} \quad (8)$$

where $\tilde{\Theta} = \Theta - \hat{\Theta}$ is the estimated parameter error vector.

In the next section, the adaptive laws that update the estimated parameter vector $\hat{\Theta}$ are developed.

IV. Adaptive Law Formulation

In this section, we shall define the adaptive law for our parameter estimator.

A. Filter design

From (2), the second state equation can be expressed as,

$$\dot{x}_2 = (A_{22}x_2 + B_{12}u_1) + \bar{B}_2\varphi\Theta + \zeta_2 \quad (9)$$

Let

$$\psi = A_{22}x_2 + B_{12}u_1 \quad (10a)$$

$$\phi = \bar{B}_2\varphi \quad (10b)$$

then, the following filtered variables can be defined as,

$$\begin{aligned} k\dot{x}_{2f} + x_{2f} &= x_2, \quad x_{2f}(0) = 0 \\ k\dot{\psi}_f + \psi_f &= \psi, \quad \psi_f(0) = 0 \\ k\dot{\phi}_f + \phi_f &= \phi, \quad \phi_f(0) = 0 \end{aligned} \quad (11)$$

where $k > 0$. In addition, we may introduce an auxiliary filter for the bounded disturbance (which is only used for analysis),

$$k\dot{\zeta}_{2f} + \zeta_{2f} = \zeta_2, \quad \zeta_{2f}(0) = 0 \quad (12)$$

i.e. $\zeta_{2f} \in L_\infty$. Consequently, we can obtain from (9) and (11) that,

$$\dot{x}_{2f} = \frac{x_2 - x_{2f}}{k}, \qquad \frac{x_2 - x_{2f}}{k} - \psi_f = \phi_f\Theta + \zeta_{2f} \quad (13)$$

B. Auxillary integrated regressor matrix and vector

The filtered variables introduced above will be used in the definition of a filtered regressor matrix, $M(t)$, and a vector, $N(t)$ as,

$$\dot{M}(t) = -k_{FF}M(t) + k_{FF}\phi_f^T(t)\phi_f(t), \quad M(0) = 0 \quad (14)$$

$$\dot{N}(t) = -k_{FF}N(t) + k_{FF}\phi_f^T(t)\left(\tfrac{x_2 - x_{2f}}{k} - \psi_f\right) \quad (15)$$

where, $k_{FF} \in \mathbb{R}^+$, can be implemented as a forgetting factor and the initial condition of $N(t)$ is $N(0) = 0$. Note that (15) is equivalent to:

$$\dot{N}(t) = -k_{FF}N(t) + k_{FF}\phi_f^T(t)(\phi_f(t)\Theta + \zeta_{2f}), \quad (16)$$

Consequently, we can find the solution to (14) and (15),

$$\begin{aligned} M(t) &= \int_0^t e^{-k_{FF}(t-r)}k_{FF}\phi_f^T(r)\phi_f(r)dr \\ N(t) &= \int_0^t e^{-k_{FF}(t-r)}k_{FF}\phi_f^T(r)\left(\tfrac{x_2 - x_{2f}}{k} - \psi_f\right)dr \end{aligned} \quad (17)$$

where

$$\begin{aligned} N(t) &= M(t)\Theta + \int_0^t e^{-k_{FF}(t-r)}k_{FF}\phi_f^T(r)\zeta_{2f}dr \\ &= M(t)\Theta + \zeta_{2N} \end{aligned} \quad (18)$$

and $\zeta_{2N} = \int_0^t e^{-k_{FF}(t-r)}k_{FF}\phi_f^T(r)\zeta_{2f}dr$. Note that ϕ is bounded since it is Lipschitz continuous and x, u_2 are bounded (Assumption 1). Thus, ϕ_f is bounded. Since $\zeta_{2f} \in L_\infty$, it follows that $N(t), M(t)$ and ζ_{2N} are bounded.

Lemma 1: The auxiliary regressor matrix $M(t) \in \mathbb{R}^{l\times l}$ is positive definite, $M(t) > 0$, if and only if $\int_0^t \phi_f^T\phi_f dt > 0$. •

Proof : It can be easily shown that

$$\begin{aligned} \int_T^t \phi_f^T(r)\phi_f(r)dr &\geq \int_T^t e^{-k_{FF}(t-r)}\phi_f^T(r)\phi_f(r)dr \\ &\geq e^{-k_{FF}t}\int_T^t \phi_f^T(r)\phi_f(r)dr \end{aligned} \quad (19)$$

when $T < t$. For $T = 0$, the claim follows. ■

Thus, if ϕ_f is persistently excited, $M(t) > \lambda_m I$ is positive definite for some $\lambda_m > 0$. Clearly, if ϕ is persistently excited for any time and a sufficiently large time interval (as derived from the linear system (11) and definition (10b)), then ϕ_f is also persistently excited [36], [34]. Thus, if ϕ is persistently excited then $M(t) > \lambda_m I$ for some $\lambda_m > 0$ and $\int_T^t \phi_f^T\phi_f dt > \lambda_m I$. In this paper, it is important to achieve $M(t) > \lambda_m I$ for our adaptation algorithm to work. This can be achieved through persistent excitation of ϕ:

Remark 1: The Persistent Excitation (PE) condition for the regressor ϕ can be achieved in the experiment through an appropriate control signal, u_1. For instance, the control signal

can be augmented by a noise signal or the controller can introduce for the system states, x, a tracking demand which achieves 'sufficient richness' (SR) of x and guarantees $M(t) > \lambda_m I, \lambda_m > 0$ as in [30]. Note also that some practical systems may be subject to sufficient disturbances causing PE, e.g. [29]. ∘

C. Parameter Estimation

We shall write our adaptive law as,

$$\dot{\hat{\Theta}} = \Gamma[\varphi^T F(y - C\hat{x}) - R(t)] \tag{20}$$

The term $R(t)$ contains a sliding mode type term to ensure fast parameter convergence,

$$\begin{aligned} R(t) &= M(t)\omega_1\Omega\frac{M(t)\hat{\Theta} - N(t)}{\left\|M(t)\hat{\Theta} - N(t)\right\|} \\ &\quad + M(t)\omega_2\Omega(M(t)\hat{\Theta} - N(t)) \end{aligned} \tag{21}$$

where ω_1 and ω_2 are positive definite scalars. Γ and Ω are positive definite and diagonal design matrices:

$$\Gamma = diag(\gamma_1, \ldots, \gamma_l),\ \Omega = diag(\omega_1, \ldots, \omega_l) \tag{22}$$

It will be proven that the parameter error matrix, $\tilde{\Theta}$, converges to zero in finite time for systems without disturbance.

Remark 2: Compared to previous results (i.e. the parameter adaptation is only driven by the observer error in (20)), the extra term $R(t)$, taking parameter error information, $M(t)\hat{\Theta} - N(t)$, is employed; this could enhance the parameter convergence performance [35]. In particular, we incorporate the sliding mode technique in (21) such that the finite-time convergence is guaranteed as stated in the next section. ∘

V. Stability and Performance

The following theorem is the key technical result which is to be applied to the mass and gradient estimation.

Theorem 1: Given a system (1), which satisfies Assumption 1-4, an adaptive observer (3) with adaptation law (20) and (14) - (15) can be designed so that the unknown parameter vector Θ can be estimated via $\hat{\Theta}$. The following holds for persistently excited ϕ (10b):

a) *Ultimate bounded stability can be satisfied for all states (observer error and parameter estimation error).*
b) *For $\zeta = 0$, the adaptive observer and parameter estimation is exponentially stable for both states (observer error and parameter estimation error).*
c) *For $\zeta = 0$, finite-time convergence of the estimated parameters can be guaranteed.*

♢

Proof : a.) Note that we assume that ϕ is persistently excited, i.e. $M(t)$ is invertible. We shall prove the ultimate boundedness at first for observer error $\tilde{x}$ and parameter estimation error, $\tilde{\Theta}$. The following Lyapunov candidate shall be employed,

$$V(t) = \frac{1}{2}\tilde{x}^T P\tilde{x} + \frac{1}{2}\tilde{N}^T M^{-1}\Gamma^{-1}M^{-1}\tilde{N} \tag{23}$$

Note that $\tilde{N} = N - M\hat{\Theta}$, i.e. $\tilde{N} = M\Theta + \zeta_{2N} - M\hat{\Theta}$ and $\tilde{\Theta} = M^{-1}[\tilde{N} - \zeta_{2N}]$. We shall then decompose (23) into,

$$\begin{aligned} V(t) &= \frac{1}{2}[\tilde{x}_1 \quad \tilde{x}_2]^T \begin{bmatrix} P_1 & 0 \\ 0 & P_2 \end{bmatrix} \begin{bmatrix} \tilde{x}_1 \\ \tilde{x}_2 \end{bmatrix} \\ &\quad + \frac{1}{2}\tilde{N}^T M^{-1}\Gamma^{-1}M^{-1}\tilde{N} \\ &= \frac{1}{2}\tilde{x}_1^T P_1\tilde{x}_1 + \frac{1}{2}\tilde{x}_2^T P_2\tilde{x}_2 \\ &\quad + \frac{1}{2}\tilde{N}^T M^{-1}\Gamma^{-1}M^{-1}\tilde{N} \\ &= V_1 + V_2 + V_3 \end{aligned} \tag{24}$$

We now analyse the functions of $V_1 = \frac{1}{2}\tilde{x}_1^T P_1\tilde{x}_1$ and $\tilde{V} = V_2 + V_3 = \frac{1}{2}\tilde{x}_2^T P_2\tilde{x}_2 + \frac{1}{2}\tilde{N}^T M^{-1}\Gamma^{-1}M^{-1}\tilde{N}$ separately for convenience. Taking the derivative of $\tilde{V}$,

$$\begin{aligned} \dot{\tilde{V}} &= \tfrac{1}{2}\left(\tilde{x}_2^T P_2\dot{\tilde{x}}_2 + \dot{\tilde{x}}_2 P_2\tilde{x}_2\right) \\ &\quad + \tfrac{d}{dt}\left[\tfrac{1}{2}\tilde{N}^T M^{-1}\Gamma^{-1}M^{-1}\tilde{N}\right] \\ &= -\tfrac{1}{2}\tilde{x}_2^T Q_2\tilde{x}_2^T + \tilde{x}_2^T P_2\bar{B}_2\varphi\tilde{\Theta} \\ &\quad + \tilde{N}^T M^{-1}\Gamma^{-1}\left(\tfrac{dM^{-1}\tilde{N}}{dt}\right) + \tilde{x}_2^T P_2\zeta_2 \\ &= -\tfrac{1}{2}\tilde{x}_2^T Q_2\tilde{x}_2^T + \tilde{x}_2^T P_2\bar{B}_2\varphi\tilde{\Theta} + \\ &\quad \tilde{N}^T M^{-1}\Gamma^{-1}\left(\dot{\tilde{\Theta}} + M^{-1}\dot{M}M^{-1}\zeta_{2N} + M^{-1}\dot{\zeta}_{2N}\right) \\ &\quad + \tilde{x}_2^T P_2\zeta_2 \end{aligned} \tag{25}$$

The matrix $\dot{M}$ (14) and the vector $\dot{\zeta}_{2N}$ (18) are bounded for bounded x_2 which implies boundedness for ζ_{BD},

$$\zeta_{BD} = M^{-1}\dot{M}M^{-1}\zeta_{2N} + M^{-1}\dot{\zeta}_{2N} \tag{26}$$

Then,

$$\begin{aligned} \dot{\tilde{V}} &= -\frac{1}{2}\tilde{x}_2^T Q_2\tilde{x}_2 + \tilde{x}_2^T P_2\zeta_2 \\ &\quad + \tilde{N}^T M^{-1}\Gamma^{-1}(\dot{\tilde{\Theta}} + \zeta_{BD}) + (\tilde{x}_2^T P_2\bar{B}_2\varphi\tilde{\Theta}) \end{aligned} \tag{27}$$

Adopting our adaptive law (20), it follows:

$$\begin{aligned} \dot{\tilde{V}} &= -\tfrac{1}{2}\tilde{x}_2^T Q_2\tilde{x}_2 + \tilde{x}_2^T P_2\zeta_2 \\ &\quad + \tilde{N}^T M^{-1}\Gamma^{-1}(-\Gamma[\varphi FC\tilde{x} - R] + \zeta_{BD}) \\ &\quad + \tilde{x}_2^T P_2\bar{B}_2\varphi\tilde{\Theta} \\ &= -\tfrac{1}{2}\tilde{x}_2^T Q_2\tilde{x}_2 + \tilde{x}_2^T P_2\zeta_2 - \zeta_{2N}^T M^{-1}\varphi FC\tilde{x} \\ &\quad + \tilde{N}^T M^{-1}R + \tilde{N}^T M^{-1}\Gamma^{-1}\zeta_{BD} \\ &= -\tfrac{1}{2}\tilde{x}_2^T Q_2\tilde{x}_2 + \tilde{x}_2^T P_2\zeta_2 - \zeta_{2N}^T M^{-1}\varphi\bar{B}_2^T P_2^T C\tilde{x}_2 \\ &\quad + \tilde{N}^T M^{-1}[M(t)\omega_1\Omega\tfrac{M(t)\hat{\Theta} - N(t)}{\left\|M(t)\hat{\Theta} - N(t)\right\|} \\ &\quad + M(t)\omega_2\Omega(M(t)\hat{\Theta} - N(t))] + \tilde{N}^T M^{-1}\Gamma^{-1}\zeta_{BD} \end{aligned} \tag{28}$$

Let $\tilde{\Omega}_1 = \omega_1\Omega$ and $\tilde{\Omega}_2 = \omega_2\Omega$,

$$\begin{aligned} \dot{\tilde{V}} &\leq -\frac{1}{2}\underline{\sigma}(Q_2)\|\tilde{x}_2\|^2 - \|\tilde{N}\|\underline{\sigma}(\tilde{\Omega}_1) \\ &\quad + \|\tilde{N}\|\bar{\sigma}(M^{-1})\bar{\sigma}(\Gamma^{-1})\zeta_{BD} \\ &\quad - \underline{\sigma}(\tilde{\Omega}_2)\|\tilde{N}\|^2 + \bar{\sigma}(P_2)\|\zeta_2\|\|\tilde{x}_2\| \\ &\quad + \|P_2\|\lambda_m^{-1}\|\zeta_{2N}\|\|\phi\|\|\tilde{x}_2\| \end{aligned} \tag{29}$$

$$\begin{aligned} &\leq -\underline{\sigma}(Q_2)\underline{\sigma}(P_2^{-1})V_2 \\ &\quad - \sqrt{2}\lambda_m\underline{\sigma}(\Gamma^{1/2})\underline{\sigma}(\tilde{\Omega}_1)\sqrt{V_3} \\ &\quad - 2\underline{\sigma}(\tilde{\Omega}_2)\lambda_m^2\underline{\sigma}(\Gamma)V_3 \\ &\quad + \sqrt{2}\bar{\sigma}(\Gamma^{-1/2})\zeta_{BD}\sqrt{V_3} \\ &\quad + \sqrt{2}\bar{\sigma}(P_2^{1/2})\varrho\sqrt{V_2} \end{aligned} \tag{30}$$

where $\varrho = 2\|\zeta_2\| + \lambda_m^{-1}\|\zeta_{2N}\|\|\phi\|$ and $\underline{\sigma}(\cdot), \bar{\sigma}(\cdot)$ denote the minimum and maximum singular values for a matrix. Note that $\zeta_{BD} \in L_\infty$ and $\varrho \in L_\infty$. Thus, the result of (30) implies that the pair $(\tilde{x}_2, \tilde{N})$ will converge to a set of ultimate boundedness. Considering the special system structure of equation (2), Assumption 2 and the boundedness of ζ_{2N}, it is easily seen that also the pair $(\tilde{x}, \tilde{\Theta})$ will enter a set of ultimate boundedness.

b.) Now, we can prove exponential stability of both states. In this case, it follows for $\zeta = 0$ and (30);

$$\begin{aligned}\dot{\tilde{V}}(t) &\leq -\frac{1}{2}\tilde{x}_2 Q_2 \tilde{x}_2 - \underline{\sigma}(\tilde{\Omega}_1)\|\tilde{N}\| \\ &\quad -\underline{\sigma}(\tilde{\Omega}_2)\|\tilde{N}\|^2 \qquad (31)\\ &\leq -\frac{1}{2}\underline{\sigma}(Q_2)\underline{\sigma}(P_2^{-1})V_2 \\ &\quad -\lambda_m^{-1}\sqrt{2}\underline{\sigma}(\tilde{\Omega}_1)\underline{\sigma}(\Gamma^{-1/2})\sqrt{V_3} \qquad (32)\\ &\quad -\sqrt{2}\lambda_m^{-2}\underline{\sigma}(\tilde{\Omega}_2)\underline{\sigma}(\Gamma^{-1})V_3\end{aligned}$$

Thus, the pair $(\tilde{x}_2, \tilde{N})$ will decay exponentially to 0. Note that, now $\tilde{N} = M\tilde{\Theta}$ and $M > \lambda_m I$. Thus, under the condition $\zeta = 0$, it follows that the pair $(\tilde{x}_2, \tilde{\Theta})$ converges exponentially to 0 and subsequently also the pair $(\tilde{x}, \tilde{\Theta})$ due to Assumption 4.

c.) To prove finite-time convergence of $\tilde{\Theta}$ for $\zeta = 0$, we can analyse $V_3 = \frac{1}{2}\tilde{N}^T M^{-1}\Gamma^{-1}M^{-1}\tilde{N}$ as follows for $M(t) > \lambda_m I$,

$$\begin{aligned}\dot{V}_3 &= \tilde{N}^T M^{-1}\Gamma^{-1}\left(-\Gamma[\varphi FC\tilde{x} - R]\right) \qquad (33)\\ &= \tilde{N}^T M^{-1}\left[-\left(\varphi FC\tilde{x} - R\right)\right] \qquad (34)\\ &= -\tilde{\Theta}^T\varphi\bar{B}_2^T P_2^T\tilde{x} + \tilde{\Theta}^T M\tilde{\Omega}_1\frac{M\hat{\Theta} - N}{\|M\hat{\Theta} - N\|} \qquad (35)\\ &\quad +\tilde{\Theta}^T M\tilde{\Omega}_2(M\hat{\Theta} - N)\\ &\leq -[\underline{\sigma}(\tilde{\Omega}_1)\lambda_m - \underline{\sigma}(P_2)\|\phi\|\|\tilde{x}\|]\|\tilde{\Theta}\| \qquad (36)\\ &\quad -\underline{\sigma}(\tilde{\Omega}_2)\lambda_m^2\|\tilde{\Theta}\|^2\end{aligned}$$

Exploiting again the fact that, $M(t) > \lambda_m I$, it follows

$$\begin{aligned}\dot{V}_3 &\leq -\frac{\sqrt{2}}{\bar{\sigma}(\Gamma^{-1/2})}[\underline{\sigma}(\tilde{\Omega}_1)\lambda_m \qquad (37)\\ &\quad -\underline{\sigma}(P_2)\|\phi\|\|\tilde{x}\|]\sqrt{V}_3\\ &\quad -\frac{2}{\bar{\sigma}(\Gamma^{-1})}\underline{\sigma}(\tilde{\Omega}_2)\lambda_m^2 V_3\end{aligned}$$

Since $\tilde{x} \to 0$ and the scalar $\|\phi\|$ is bounded, there is a time T_1 where, for $t > T_1$

$$\underline{\sigma}(\tilde{\Omega}_1)\lambda_m > \underline{\sigma}(P_2)\|\phi\|\|\tilde{x}\| \qquad (38)$$

Thus, there is a time T_2 so that for $t > T_2$ and $\epsilon > 0$: $\dot{V}_3 \leq -\epsilon\sqrt{V_3}$. Hence, using results from [25] finite-time convergence of the parameter error $\tilde{\Theta}$ to zero can be achieved. ■

Remark 3: The result in Theorem 1 in fact is quite generic. It also allows for analysis of measurement errors of x_2 and ϕ. For this reason, we may have in the observer some measurement errors affecting both x_2 and also $\varphi(x, u_2)$ measurement and in reality $\check{x}_2$ and $\check{\varphi}(x, u_2)$ are provided in the practical system. Thus, the observer equation is

$$\dot{\hat{x}} = A\hat{x} + B_1 u_1 + B_2\check{\varphi}\hat{\Theta} + L(\check{x}_2 - C\hat{x}) \qquad (39)$$

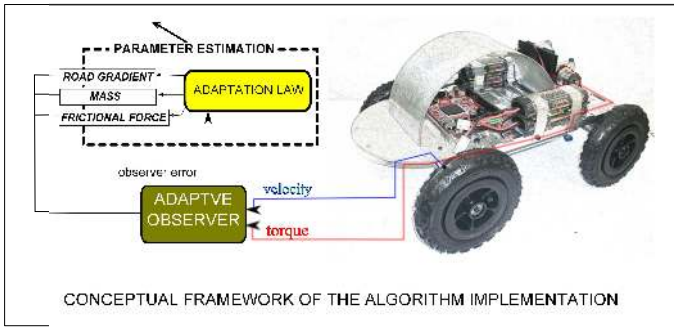

CONCEPTUAL FRAMEWORK OF THE ALGORITHM IMPLEMENTATION

Fig. 1. Parameter Estimation Algorithm Implementation Concepts

The plant dynamics in (9) can be rewritten as,

$$\begin{aligned}\dot{\check{x}} &= (A\check{x} + B_1 u_1) + B_2\check{\varphi}\Theta + \zeta + (\dot{\check{x}} - \dot{x})\\ &\quad +A(x - \check{x}) + B_2(\varphi - \check{\varphi})\Theta\end{aligned} \qquad (40)$$

where $\check{x} = [x_1^T \quad \check{x}_2^T]^T$. Assuming the measurement errors and its derivative are bounded, (i.e. $(x-\check{x}), (\dot{x}-\dot{\check{x}}), (\varphi-\check{\varphi}) \in L_\infty$), so that $\check{x}_2, \dot{\check{x}}_2 \in L_\infty$, then the plant dynamics (9) are,

$$\dot{\check{x}} = (A\check{x} + B_2 u_1) + B_2\check{\varphi}\Theta + \check{\zeta} \qquad (41)$$

where

$$\check{\zeta} = \zeta + (\dot{\check{x}} - \dot{x}) + A(x - \check{x}) + B_1(\varphi - \check{\varphi})\Theta \qquad (42)$$

can be regarded as a bounded disturbance. Defining the error dynamics as $\tilde{\check{x}} = (\check{x} - \hat{x})$ it follows that,

$$\dot{\tilde{\check{x}}} = A_c\tilde{\check{x}} + B_2\check{\varphi}\Theta + \check{\zeta} \qquad (43)$$

Under the assumption that $\check{\zeta}$ is bounded, we can continue the analysis as for Theorem 1. Further discussions are omitted here due to space reasons. ◦

VI. Parameter Estimation in the Vehicle Dynamics

In this section, we will discuss the previously formulated parameter estimation algorithm in the context of its application to road gradient and vehicle's weight estimation. The concept of the proposed algorithm application can be depicted in Figure 1 where only velocity and torque of the vehicle are needed as inputs to the estimation algorithm. Figure 2 shows the simplified model of the small-scaled model car used in the experiment to validate the parameter estimation algorithm.

A. Vehicle model

The parameters to be estimated are the road inclination, θ, on which the vehicle traverses, the mass of the vehicle, m and the viscous friction coefficient, C_{vf}. Referring to Figure 2, assuming the air drag F_{drag} is negligible at low speeds[1] below $0.2\ m/s$ and the braking force F_{brake} is subsumed in the driving force, F_{engine}, we may model the small-scaled model car using Newton's Second Law in the longitudinal direction to yield,

$$m\ddot{x} = F_{engine} - mgsin(\theta) - C_{vF}\dot{x} - C_\mu mgcos(\theta) \qquad (44)$$

[1]In real-sized vehicles, the air drag cannot be neglected. In this case, the term F_{drag} will have to be estimated in a similar way as presented for the other forces below. Relevant detail is avoided here due to space reasons.

where m is the mass of the vehicle, θ is the road gradient on which the vehicle traverses, $\dot{x}$ is the vehicle's velocity, C_{vF} is the viscous damping/friction coefficient and C_μ is the rolling friction coefficient. Adhering to the structure presented in (1), we may represent the system in the following state space representation,

$$\begin{aligned}\begin{bmatrix}\dot{x}\\ \ddot{x}\end{bmatrix} &= \begin{bmatrix}0 & 1\\ 0 & 0\end{bmatrix}\begin{bmatrix}x\\ \dot{x}\end{bmatrix}+\begin{bmatrix}0\\ \frac{1}{m}\end{bmatrix}F_{engine}- \\ &\quad \begin{bmatrix}0\\ sin\theta + C_\mu cos\theta\end{bmatrix}g-\begin{bmatrix}0\\ \frac{C_{vF}}{m}\end{bmatrix}\dot{x} \qquad (45)\\ y &= \begin{bmatrix}1 & 0\\ 0 & 1\end{bmatrix}\begin{bmatrix}x\\ \dot{x}\end{bmatrix}\end{aligned}$$

which will be used to develop our extended adaptive parameter estimator.

B. Observer Design

Following the general structure presented in (3), the adaptive observer with finite-time parameter estimation can be written as,

$$\begin{aligned}\dot{\hat{\mathbf{x}}} &= A\hat{\mathbf{x}}+\begin{bmatrix}0\\ 1\end{bmatrix}[-g \quad F_{engine} \quad -\dot{x}]\begin{bmatrix}\hat{s}\\ \hat{b}\\ \hat{f}\end{bmatrix} \qquad (46)\\ &\quad +L(y-\hat{y})\\ y &= C\hat{\mathbf{x}} \qquad (47)\end{aligned}$$

where $\hat{\mathbf{x}} = [\hat{x} \quad \dot{\hat{x}}]$ is the observed state vector. The observer's system matrix, A and its output matrix, C are defined as

$$A = \begin{bmatrix}0 & 1\\ 0 & 0\end{bmatrix}, \quad C = \begin{bmatrix}1 & 0\\ 0 & 1\end{bmatrix} \qquad (48)$$

$\hat{s}$, $\hat{b}$, $\hat{f}$ are the estimated parameters of $sin\theta + C_\mu cos\theta$, $\frac{1}{m}$ and $\frac{C_{VF}}{m}$ respectively whereas L is the observer gain chosen to deliver the positive definite Lyapunov matrix P such that it satisfies (4). The engine driving force F_{engine} is assumed to be bounded (as it implements a velocity controller) to ensure that the system states x remain bounded. Thus, using this structure, it follows,

$$B_2 = \begin{bmatrix}0\\ 1\end{bmatrix}, \quad \hat{\Theta} = \begin{bmatrix}\hat{s}\\ \hat{b}\\ \hat{f}\end{bmatrix}, \quad \varphi = \begin{bmatrix}g\\ F_{engine}\\ \dot{x}\end{bmatrix}^T \qquad (49)$$

The observer adaptive weights are lumped such that,

$$\Gamma = diag(\gamma_s, \gamma_b, \gamma_f), \quad \Omega = diag(\omega_s, \omega_b, \omega_f) \qquad (50)$$

VII. Practical Application Results

This section presents the practical implementation of our proposed novel estimation algorithm. The hardware realisation is briefly described at first followed by the estimation performance characterisation methodology. This section elucidates the method to assess the performance of the algorithm. The Mean Integral Absolute Error (mean IAE), which will be explained is used in the characterisation as a performance index computed across different sets of test condition (various slope profiles) and settings (noise level and velocity variations). Results on road gradient estimation performance are discussed which are then followed by mass estimation results.

A. Hardware implementation

A previously built small-scale model car [27] was used in the experiment to evaluate the estimation algorithm. There were two parameters to be estimated:- the vehicle's mass (nominally weighs $\sim$ 10kg) and the road gradients on which it traverses. An inclinometer, SCA61T, was installed for gradient measurements solely for reference purpose and not to be used in the algorithm. Figure 3 shows the implemented controller system network and architecture which emulates the system network of a road vehicle.

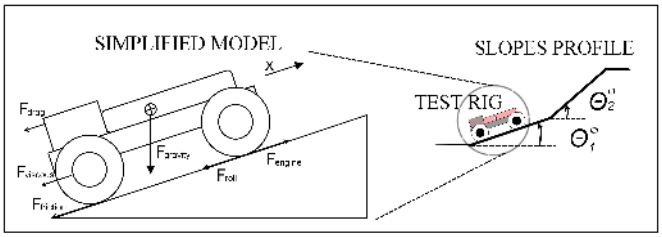

Fig. 2. Simplified model of the small-scaled model car and the slope profile

TABLE I
Tested Slope Profile

Slope profile	θ_1	θ_2
1	10°	15°
2	18°	0°
3	15°	20°
4	22.3°	11.8°

TABLE II
Characterisation through variation in Noise and velocity Demand

	Experimental set for variation in noise					
set	1	2	3	4	5	6
noise	×2	×4	×8	×10	×20	×40

	Experimental set for variation in velocity demand [m/s]						
set	7	8	9	10	11	12	13
velocity	0.1	0.12	0.14	0.18	0.2	Sines	Steps

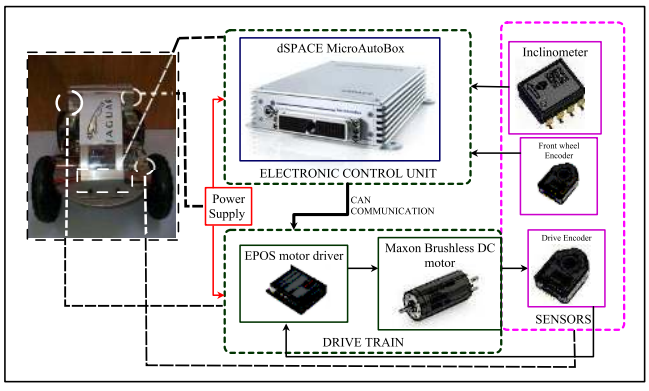

Fig. 3. Functional Structure of the System Onboard

Together with Matlab^{TM}, the dSPACE MicroAutoBox, used in the experiment, is a dedicated Rapid Prototyping embedded

system suited to test the proposed estimation algorithm. The drive train comprises of an EPOS 24/5 motor driver and the brushless DC motor (EC-i 40 Maxon) representing the vehicle's engine. The motor is current-controlled via the MicroAutoBox which subsequently provides the driving force, F_{engine}, proportional to the current signal, being controlled. Two Agilent HEDL5540 encoders are installed, one is attached to the driving motor and the other one is attached to the front wheel which is passive and not coupled to the drive train. The reasons for such attachment are two-fold. The first reason is to provide the true speed measurement of the vehicle. Secondly, they were used to help us in monitoring any sign of slippage on the rear driving wheel which may be caused by the excessive jerkiness or acceleration by the motor due to over excitation of the control signal. In our experiment, we would avoid the occurrence of significant slippage as this would invalidate our estimation effort. The tyre pressure of the test rig is kept at a reasonably high value to allow true velocity measurement, i.e. introducing fairly stiff tyres. Slippage was avoided by keeping vehicle acceleration/velocity limited.

The test slope rig, constructed from two stiff wooden planks of 2 m in length each, were tilted and bolted together to give various slope profiles (Figure 2). There were four slope profiles (Table I) chosen to characterise the performance of our novel estimation algorithm. The starting slope would be always zero, i.e. flat ground start-up. Two load masses (of 1.85kg each) were used in the experiment to evaluate the mass estimation performance of the proposed algorithm on a flat surface.

B. Methodology

Tests were carried out in accordance to different segments of the designated slope profile (Table I) to investigate the effectiveness of our novel estimation algorithm across different road gradients. The following cardinal performance measures are outlined to evaluate the proposed novel algorithm:

- Algorithm effectiveness in the presence of deliberate injection of white noise of different levels to the control signal i.e. the torque to the engine with purpose to aid the learning.
- Effects on the convergence of the parameter estimation for different levels of vehicle's traversal velocity and demand signal.
- Algorithm effectiveness in mass estimation

Referring to Table II, characterisation tests were carried out requiring the small-scaled model car to traverse up the designated slope at various constant velocity ranges from 0.1 m/s till 0.2 m/s followed by a demand with sinusoidal variation containing two distinct frequencies ($y[m/s] = 0.15 + 0.01sin(0.5t) + 0.01sin(t) + 0.01cos(0.25t)$) and a Step type velocity demand signal ranging between $0.14 \sim 0.17$ m/s. Table II also shows various levels of white noise injected into the control signal for PE condition enhancement. Figure 2 shows the simple model depicting the dynamics of the vehicle and the generic test slope profile representation. The mean Integral Absolute Error (IAE) is computed by taking the sums of absolute error between the inclinometer reading and the estimated road gradient and divide the sums by the discrete time unit (nT), i.e.

$$E_{I\bar{A}E} = \frac{\sum_{nT} \|\theta_{inclinometer} - \theta_{estimated}\|}{nT} \tag{51}$$

This is used as the performance index to characterise the algorithm's performance over various levels of noise and different types of velocity demands across the designated slope profiles (Table I). The performance, marked by the computed mean IAE, of our proposed novel algorithm will be compared against the conventional least-square based algorithm (equivalently setting the term $R(t) = 0$). Another useful performance index used in the experiment was the condition number of $M(t)$. A low condition number is favored (ideal numerical value is 1) as this signifies that the system is Persistently Excited. A sampling rate of $T_s = 0.0008s$ was used throughout the experiment.

Remark 4: It is to note that for real-sized vehicles, the torque originated from the engine may already contain a persistently exciting signal. Thus, the need for artificial excitation signals might be removed. In addition to varying road surface conditions, the driver's behaviour may also introduce PE condition. Small continuous changes of velocity may provide sufficient information for identification. It is well known that practical "real-life" conditions can enhance the performance of adaptation algorithms, e.g. [29]. ∘

C. Parameter tuning

In our experiment, there were important parameters (see Table III) of the adaptive observer algorithm needed to be tuned to achieve satisfactory results. It is to be noted that universal adaptation gains and tuning knobs were obtained via the Lyapunov design, achieved in the preceding Section V. For practical implementation, the algorithm of (20) was slightly modified and a projection method [21] was introduced to limit the parameter values via realistic lower and upper bounds (Table IV). Assuming the algorithm is stable, it will remain within the bounds and avoid hitting them most of the time. This will be discussed later in the practical tests. In particular, we will be interested in a performance index $\bar{\hat{m}}\%$ which represents the ability of the algorithm to stay away from the practically imposed bounds. It can be calculated by

$$\bar{\hat{m}}\% = \frac{t_b}{t_d} 100 \tag{52}$$

where t_b is the sum of the periods of the estimated mass touching the bounds, divided by the overall estimation period, t_d. The forgetting factor, k_{FF} which corresponds to the auxiliary regressors (formulated in Section IV-B equation (14) and (15)) was chosen to prevent the regressor matrix from growing unboundedly, compromising the need for conserving the immediate past horizon data (for better learning) and at the same time, ensuring faster parameter convergence. The corresponding values of the parameters displayed in the table are used in the experiment. Figures 4(a) and 4(b) show the effects of estimation performance (measured by mean IAE) of varying the adaptation gains γ_s, γ_b (see Equation (50)). As shown in Figure 4(a), increasing γ_s enhances the gradient estimation performance as this adaptive weight is associated with the gradient term, $(sin\theta)$. On the other hand,

TABLE III
ADAPTATION MECHANISM PARAMETERS

Parameter Description	Symbols	Values
Observer Adaptive weights, Γ	γ_1	700
	γ_2	10
	γ_3	100
Sliding-Mode Adaptive weights, Ω	ω_s	3.2×10^{-15}
	ω_b	1×10^{-15}
	ω_f	0.18
Adaptation Gain within the leakage term, R	ω_1	13.5
	ω_2	0.5
Forgetting Factor	k_{FF}	0.5
Filter Poles	k	0.001

TABLE IV
SATURATION LIMITS

Plant Parameters	Estimation	Lower Limit	Upper Limit
Mass(m,kg)	$\hat{m}$	10	20
	$\hat{b} = 1/\hat{m}$	0.05	0.1
Gradient(θ,°)	$\hat{\theta}$	-20	20
	$sin(\hat{\theta})$	-0.5	0.5
Friction Coefficient	C_{VF}	0	1
(C_{VF},kg/s)	$\hat{f} = C_{VF}/\hat{m}$	0	0.1

γ_b, associated with the mass estimation and correlated with the engine force, needs to be selected at a right magnitude so as to have the algorithm sufficiently sensitive to changes in gradient but not to over-excite the adaptation. The adaptation gains associated with the leakage term, R (see Equation (21)) comprised of ω_1 and ω_2 which are constant scalars chosen to be sufficiently large by virtue of Lyapunov Design as analysed in Section V. It is also evident in Figure 4(c) that there is a compromise in selecting ω_1 to be significantly larger than ω_2 to drive the estimated parameters to the true values in finite-time. Having ω_1 too large may subject the algorithm to be over-sensitive to noise. For instance, the over-sensitised algorithm to noise and system changes at high magnitude of ω_1 shows a sharp spike during the track gradient transition. It is apparent to observe the term ω_1 works in concert with ω_2, whereby, adhering to the requirement of a sufficiently large ω_1, a lower ω_2 improves the convergence rate.

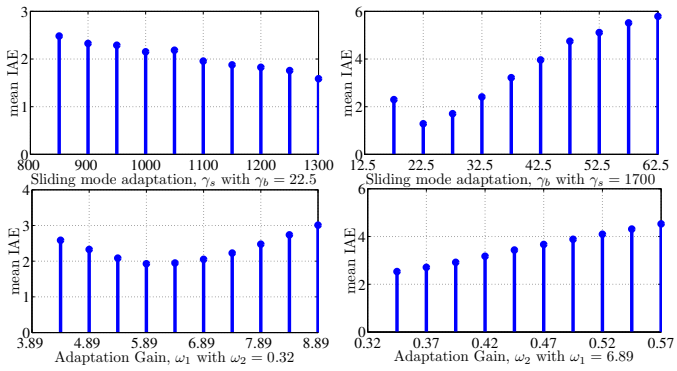

Fig. 4. Effects on the estimation performance by tuning (a) γ_s, (b) γ_b, (c) ω_1 and (d) ω_2.

D. Determination of Rolling Friction Coefficient, C_μ

Another component of the vehicle's dynamic model required to be known is the rolling friction coefficient, C_μ. This was determined by allowing the vehicle to traverse in a constant velocity on a flat surface, i.e. $\theta = 0$, thereby the algorithm would estimate $\hat{C}_\mu$ with a notion that $sin\theta = 0$ and $cos\theta = 1$ were kept constant. The surface material on which the vehicle was tested was of cement floor type. The value of $\hat{C}_\mu$ was found to be in the range of $0.1 \sim 0.15$. The value $C_\mu = 0.12$ was employed as a known constant in the dynamic model. Hence, the algorithm would be then used to estimate the road gradient.

E. Road Gradient Estimation

Road gradient estimation performance will be evaluated under two sets of settings:- i.) different levels of noise content in the control signal and ii.) different velocity profiles.

1) Influence of noise content in the control signal on the estimation performance: Figure 5 shows the distribution of computed mean IAE across four types of slope profiles for various levels of magnitude of white noise injected into the control signal. From the figure, it clearly shows that a white noise multiplied by 8 times of the nominal level enhanced the estimation.

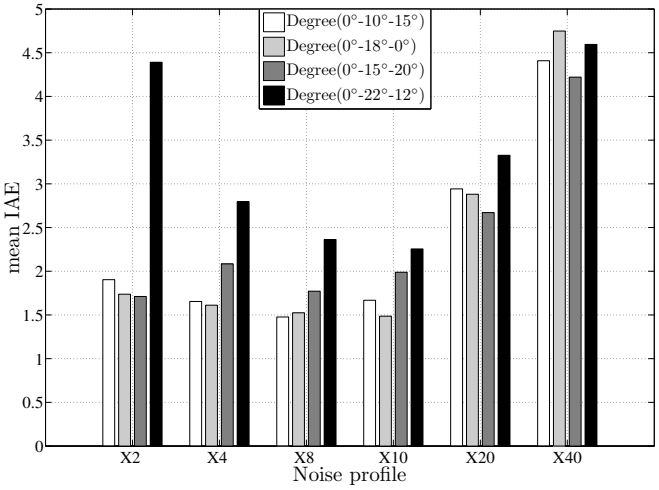

Fig. 5. Mean IAE distribution for all slope profiles with different level of noise multiplier

2) Influence of the velocity profile in the control signal on the estimation performance: Using the characterisation result from Section VII-E1, the optimal noise level (8 times of nominal) is used in this section. Figure 6 shows the distribution of computed mean IAE for different velocity level and demand type across four types of slope profile. The figure also shows that 0.14 m/s would be the optimal velocity for the algorithm to best perform. Having this knowledge at our expense, the proposed algorithm was compared with the conventional least-square (LS) based algorithm [1], [24], [13], [20], [19] across all four types of slope profiles. Estimation performance results for two slopes are shown in Figure 7 and 9. Figure 10 also shows that our proposed algorithm supersedes the LS

algorithm in terms of the performance index, $\bar{\hat{m}}\%$ (52). Figure 8 shows that all the three estimated components, i.e. $\hat{s}, \hat{b}$ and $\hat{f}$ remained within the realistic practical bounds. Interestingly, $\hat{f}$, associated with the coefficient of viscous friction, $\hat{C}_{vf}$, remained constant in between $0.015 \sim 0.02$. Assuming the nominal mass of the vehicle was 10 kg, this translates to having $\hat{C}_{vf} \approx 0.2$ which is of an acceptable value.

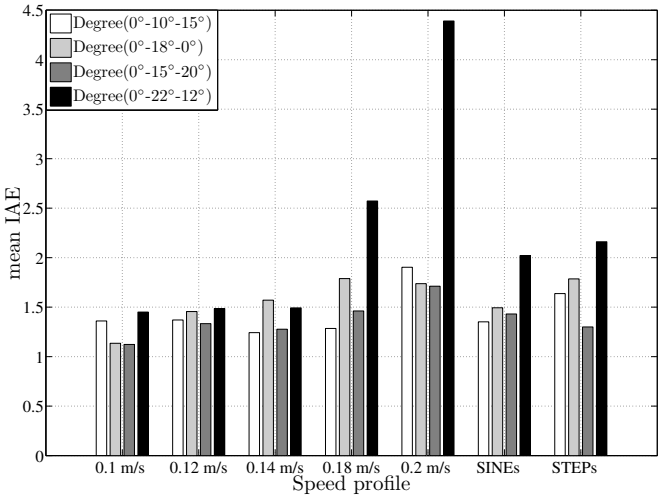

Fig. 6. Mean IAE distribution for all slope profiles with various velocity demand

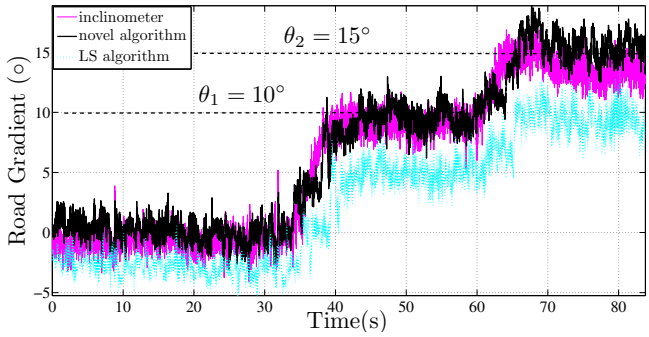

Fig. 7. Comparative gradient estimation for slope profile 1 with the optimal velocity at 0.14 m/s

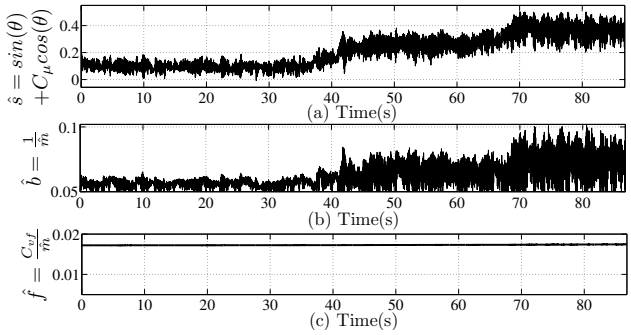

Fig. 8. The estimated parameter components, (a) $\hat{s}$, (b) $\hat{b}$ and (c) $\hat{f}$ during the gradient estimation of a slope with slope profile 1

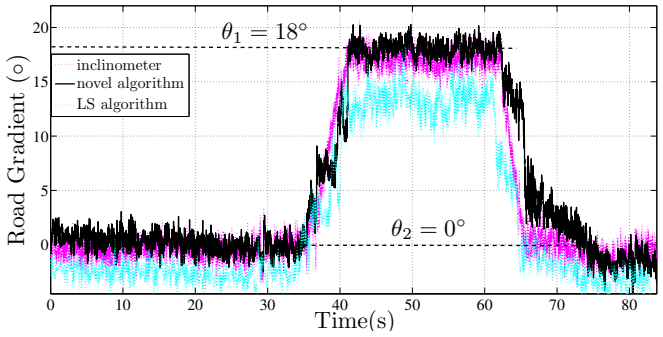

Fig. 9. Comparative Gradient estimation for slope profile 2 with the optimal velocity at 0.14 m/s

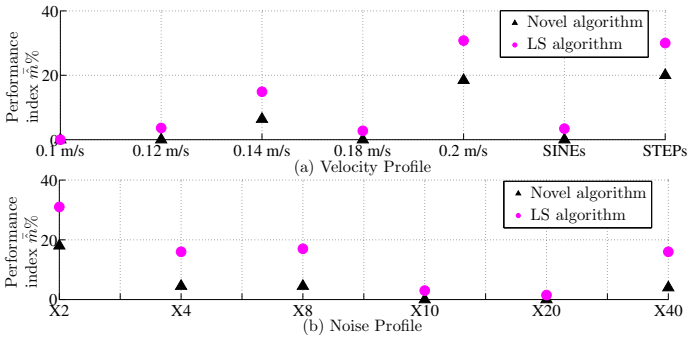

Fig. 10. Percentage of hitting the mass estimation limit during the traverse for Slope profile 1 with (a) velocity variations and (b) noise level variations

F. Mass Estimation Performance

A test was also carried out to evaluate the performance of the proposed estimation algorithm in estimating the step changes of mass on the vehicle. This is, in reality, equivalent to the unloading of cargo boxes or passengers from a truck or a SUV(sports utility vehicle) vehicle (See section VII-D for test procedure to determine C_μ). Figure 11 shows the estimated mass of the vehicle together with the preloaded masses. The original signal of the estimated mass (shown by the lighter (vigorous) shades of the plot) was filtered by a Butterworth low pass filter with a 3 rad/s cut-off frequency. The test rig

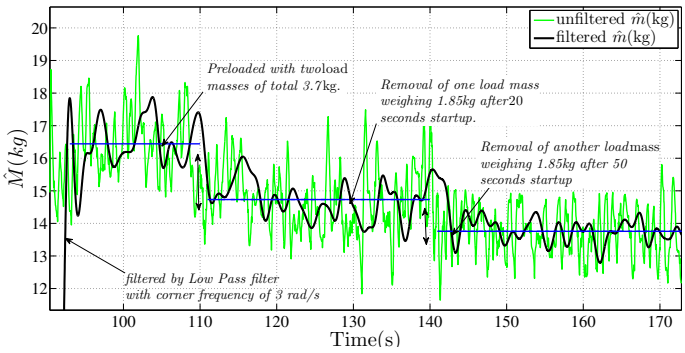

Fig. 11. Mass Estimation,$\hat{m}$ (kg)

was preloaded with two extra load masses, weighing each 1.85 kg giving a total mass of 13.70 kg (since the net mass of the vehicle is 10 kg). Then, two load masses of 1.85 kg were removed consecutively at two intervals. The load masses

were placed (at the initial position) at almost center position to allow equal distribution of mass addition on the test rig. The vehicle was controlled to travel on a flat ground with constant velocity of 0.14 m/s assuming a constant rolling friction was present. White noise was also injected to the control signal supplied to the motor for regulated PE condition. The choice of the noise multiplier level and suitable traversal velocity were based on the test conducted in the previous road gradient performance characterisation test. Figure 11 shows that the novel estimation algorithm is sufficiently sensitive to the changes in the vehicle's mass, awarding a very good mass estimation performance in its trait. Owing to the sliding-mode term in the adaptive law of the proposed estimation algorithm, the performance concurs with the initial theory and analysis in terms of its guaranteed finite-time convergence feature. Again, the finite-time convergence can be only ensured if (14) and (15) satisfy the PE condition. The result shows relatively good performance in terms of its responsiveness and accuracy. To strain the estimation effort further, the integrator of the algorithm's filtered regressor were reset at the time of load masses removal with a purpose to see the convergence effect on it. Figures 12-13 show the effects of resetting the integrators and remarkably that the estimation was responsive to settle at the true value within a short time as proven in the theory by virtue of Lyapunov analysis. Hence, the results of Figure 11 are not influenced by the resetting or lack of resetting of the filtered regressor matrix (14) and vector (15) during experimentation.

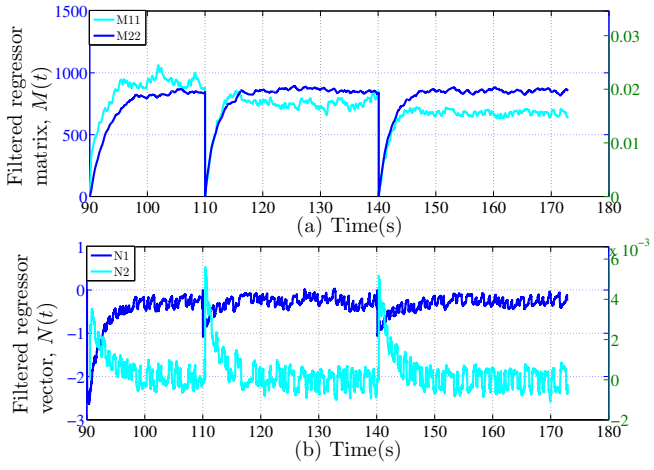

Fig. 12. Filtered Regressor (a) Matrix, $M(t)$ and (b) Vector, $N(t)$

G. Effects of Viscous Friction, C_{vf}, and Persistent Excitation

Prudent observation of the behavior of the estimated parameters in the experiment revealed that the viscous friction component, C_{vf}, imposed an insignificant influence on the overall dynamic of the system. Hence, the estimation performance would not be adversely affected by the component. Figure 8 (c) shows the key component associated with C_{vf}, i.e. $\hat{f}$. It displays a constant value without much erratic behaviour. To investigate the rationale behind the phenomena, Table V illustrates the numerical disparity of $\hat{C}_{vf}$ in terms of its

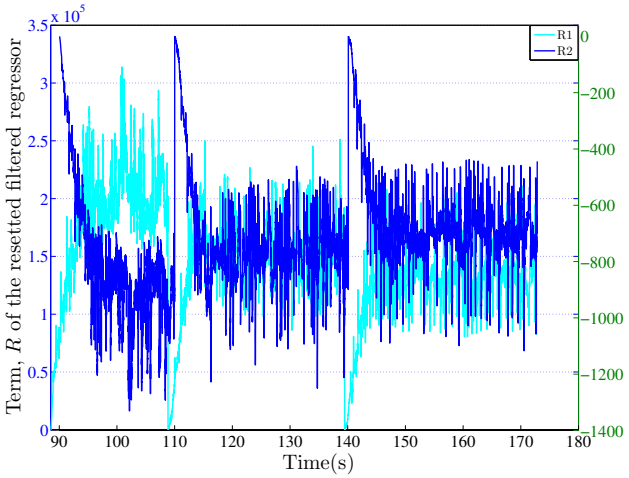

Fig. 13. Term R(t) in (21), R_1 (dark blue & right hand axis), R_2 (light blue & left hand axis)

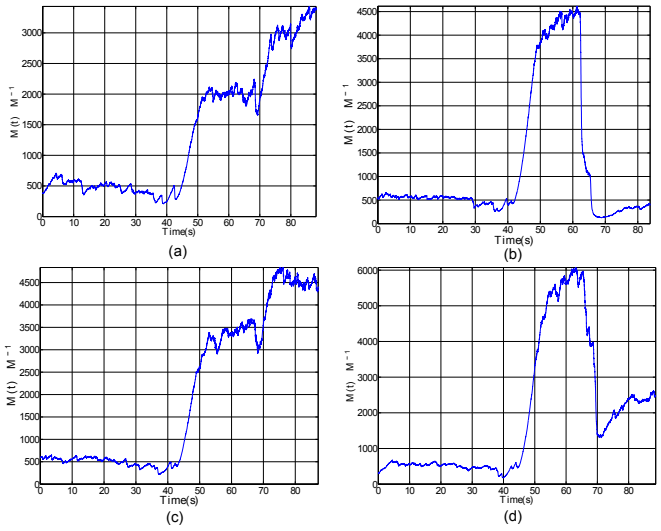

Fig. 14. Condition Number of filtered regressor, (14) for (a) slope profile 1, (b) slope profile 2, (c) slope profile 3 and (d) slope profile 4.

dynamic effect in comparison to the rest of the components, in particular, F_{engine}. Observing the dynamic contribution of $\hat{C}_{vf}$ in both extremities, the magnitude of $\hat{f} \cdot \dot{x}$ is very small in comparison to the rest of the key dynamic components such as $(sin\theta + C_\mu) \cdot g$ and $\frac{1}{m} \cdot F_{engine}$. Referring back to Section VII-E2, $\hat{C}_{vf}$ is estimated to be approximately 0.2, and the velocity was set at 0.14 m/s. The computed condition number of the filtered regressor matrix in (14) with all the three regressors involved (F_{engine}, g, $\dot{x}$) is about 1×10^7 which is very high. A very high condition number indicates that the regressor, $\dot{x}$, in particular, has either a strong correlation with any of the two regressors, possibly regressor g, i.e. gravity or the magnitude of the regressor value is insignificant. In this case, the huge difference in magnitude of $\dot{x}$ and F_{engine} explains this ill-conditioning of the filtered regressor matrix as the filtered regressor matrix involves the squaring of these disparate regressors.

TABLE V
THE MAGNITUDE OF VISCOUS FRICTION, $\hat{C}_{vf}$ IN COMPARISON WITH OTHER DYNAMIC COMPONENTS

$\ddot{x} = -sin\theta \cdot g - C_\mu \cdot cos\theta \cdot g + \frac{1}{m} \cdot F_{engine} - \frac{C_{vf}}{m} \cdot \dot{x}$				
	Component values at two extremities			
Extremity	$sin\theta \cdot g$	$C_\mu \cdot cos\theta$	$\frac{1}{m} \cdot F_{engine}$	$\frac{C_{vf}}{m} \cdot \dot{x}$
Upper bounds	4.27	0.09	6	0.002
Lower bounds	0.974	0.1	2	0.0028

Therefore, in retrospect, the PE condition of (14) should be investigated by computing the condition number of the filtered regressor, (14), involving only two key regressors, g and F_{engine}. Velocity, v, which relates to the viscous friction, was omitted from the filtered regressor matrix in (14). This creates a well conditioned filtered regressor matrix with a condition number of about 3000. This verifies that the PE condition has been fulfilled in this case. Figure 14 shows the respective condition number computed for experiments involving all slope profiles. Hence, the PE condition is fulfilled for all the experiments. The results without the inclusion of C_{vf} into the model and estimation are in fact fully consistent with the results where the C_{vf} estimation was included (see prior sections).

VIII. ACKNOWLEDGMENT

This work is supported by a joint grant between the Royal Society UK and National Natural Science Foundation of China under Grant No. JP090823/61011130163 and the National Natural Science Foundation of China under Grant 61203066 and Grant 61273150. The first author would like to thank Universiti Sains Malaysia and the Ministry of Higher Education of Malaysia for his PhD programme sponsorship. The authors are also particularly thankful to dSPACE Inc. for their provision of the MicroAutobox.

IX. CONCLUSION

An adaptive observer with novel sliding-mode based parameter estimation algorithm to estimate the road gradient and vehicle's mass is presented. The proposed parameter estimator with the sliding-mode term has been proven analytically to be finite time convergent to an error of well defined bound. The algorithm shows significant levels of robustness to disturbances and a particular class of measurement errors. The analytical results are further supported and validated by the practical implementation in a form of experiments conducted on a small-scale vehicle traversing a designated test slope profile with certain parameters tuned. Performance characterisation has been conducted to evaluate the effectiveness of the proposed road gradient estimation algorithm given a certain level of noise introduced in the control signal and under a certain traversal velocity. The practical results show a significant improvement over the LS-based algorithm in terms of realistic values within the physical bounds and convergence.

REFERENCES

[1] H. Bae, J. Ryu, and J. Gerdes, "Road grade and vehicle parameter estimation for longitudinal control using gps," in *IEEE Conference on Intelligent Transportation Systems, Proceedings, ITSC*, 2001, pp. 166–171.

[2] H. Jansson, E. Kozica, P. Sahlholm, and K.-H. Johansson, "Improved road grade estimation using sensor fusion," in *Proceedings of the 12th Reglermote in Stockholm, Sweeden*, 2006.

[3] P. Sahlholm and K. Johansson, "Segmented road grade estimation for fuel efficient heavy duty vehicles," in *IEEE Conference on Decision and Control*, 2010.

[4] M. McIntyre, T. Ghotikar, A. Vahidi, X. Song, and D. Dawson, "A two-stage lyapunov-based estimator for estimation of vehicle mass and road grade," *IEEE Transaction on Vehicular Technology*, vol. 7, no. 7, pp. 3177–3185, September 2009.

[5] S. Mangan and J. Wang, "Development of a novel sensorless longitudinal road gradient estimation method based on vehicle can bus data," *Mechatronics, IEEE/ASME Transactions on*, vol. 12, no. 3, pp. 375 – 386, 2007.

[6] V. Winstead and I. Kolmanovsky, "Estimation of road grade and vehicle mass via model predictive control," in *Control Applications, 2005. CCA 2005. Proceedings of 2005 IEEE Conference on*, 2005, pp. 1588 –1593.

[7] A. Vahidi, M. Druzhinina, A. Stefanopoulou, and H. Peng, "Simultaneous mass and time-varying grade estimation for heavy-duty vehicles," in *American Control Conference, 2003. Proceedings of the 2003*, vol. 6. IEEE, 2003, pp. 4951–4956.

[8] R. Daily and D. Bevly, "The use of gps for vehicle stability control systems," *IEEE Transaction on Industrial Electronics*, vol. 51, no. 2, pp. 270–277, April 2004.

[9] J. Stephant, A. Charara, and D. Meizel, "Virtual sensor: Application to vehicle sideslip angle and traversal forces," *IEEE Transaction on Industrial Electronics*, vol. 51, no. 2, pp. 278–289, April 2004.

[10] Y. Hori, "Future vehicle driven by electricity and control-research on four-wheel-motored "uot electric march ii"," *IEEE Transaction on Industrial Electronics*, vol. 51, no. 5, pp. 954–962, October 2004.

[11] W. Wang, I. Li, M. Chen, S. Su, and S. Hsu, "Dynamic slip-ratio estimation and control of antilock braking systems using an observer-based direct adaptive fuzzy-neural controller," *IEEE Transaction on Industrial Electronics*, vol. 56, no. 5, pp. 1746–1756, May 2009.

[12] R. Frampton and P. Thomas, "Effectiveness of electronic stability control systems in great britain," Department for Transport, VSRC, Loughborough, Tech. Rep., March 2007, report prepared for the Department for Transport.

[13] H. Fathy, D. Kang, and J. Stein, "Online vehicle mass estimation using recursive least squares and supervisory data extraction," in *American Control Conference*, Westin Seattle Hotel, Seattle, Washington, USA., June 2008.

[14] P. Sahlholm and K. Johansson, "Road grade estimation for look-ahead vehicle control using multiple measurement runs," *Control Engineering Practice*, vol. 18, no. 11, pp. 1328 – 1341, 2010.

[15] P. Lingman and B. Schmidtbauer, "Road slope and vehicle mass estimation using Kalman filtering," *Vehicle System Dynamics*, vol. 37, pp. 12–23, 2002.

[16] J. Park, J. Kong, H. Jo, Y. Park, and J. Lee, "Measurement of road gradients for the development of driving modes including road gradients," in *Proc. Inst. Mech. Eng. Automob*, vol. 215, no. D9, 2001, pp. 997–986.

[17] S. Mangan, J. Wang, and Q. Wu, "Measurement of the road gradient using an inclinometer mounted on a moving vehicle," in *IEEE Inter-national Symposium on Computer Aided Control System and Design*, 2002.

[18] J. Barrho, M. Hiemer, U. Kiencke, and T. Matsunaga, "Estimation of elevation difference based on vehicle's inertial sensors," in *16th IFAC World Congress in Praque*. IFAC, July 2005.

[19] A. Vahidi, A. Stefanopoulou, and H. Peng, "Recursive least squares with forgetting for online estimation of vehicle mass and road grade: theory and experiments," *International Journal of Vehicle Mechanics and Mobility*, vol. 43:1, pp. 31–55, 2005.

[20] ——, "Experiments for online estimation of heavy vehicle's mass and time-varying road grade," in *Proceedings IMECE, Jan 2003*, 2003.

[21] P. Iaonnou and J. Sun, *Robust Adaptive Control*. Prentice Hall, 1996.

[22] V. Adetola and M. Guay, "Finite-Time Parameter Estimation in Adaptive Control of Nonlinear Systems," *IEEE Transactions on Automatic Control*, vol. 53, no. 3, pp. 807–811, Apr. 2008. [Online]. Available: http://dx.doi.org/10.1109/TAC.2008.919568

[23] ——, "Performance Improvement in Adaptive Control of Linearly Parameterized Nonlinear Systems," *IEEE Transactions on Automatic Control*, vol. 55, no. 9, pp. 2182–2186, Sep. 2010. [Online]. Available: http://dx.doi.org/10.1109/TAC.2010.2052149
[24] S. Bittanti, P. Bolzern, and M. Campi, "Recursive Least-Square Identification Algorithms with Incomplete Excitation: Convergence Analysis and Application to adaptive control," *IEEE Transactions on Automatic Control*, vol. 35, no. 12, pp. 1371–1373, Dec. 1990.
[25] S. P. Bhat and D. S. Bernstein, "Continuous Finite-Time Stabilization of the Translational and Rotational Double Integrators," vol. 43, no. 5, pp. 678–682, 1998.
[26] C. Edwards and S. Spurgeon, *Sliding mode control: theory and applications*. CRC, 1998.
[27] J. Foreman, M. Yazdouni, S. Russo, G. Chan, A. Spiers, G. Herrmann, and P. Barber, "Hardware in the loop validation of a gradient and weight estimation algorithm and longitudinal speed control using a laboratory model car," in *International Conference on Systems Engineering (ICSE)*, 2009.
[28] R. Frampton and P. Thomas, "Effectiveness of electronic stability control systems in great britain," Department for Transport, Vehicle Safety Research Centre (VSRC), Loughborough, Tech. Rep., March 2007, report prepared for the Department for Transport.
[29] G. Herrmann, S. Ge, and G. Guo, "Discrete linear control enhanced by adaptive neural networks in application to a hdd-servo-system," *Control Engineering Practice*, vol. 16, no. 8, pp. 930 – 945, 2008.
[30] J. Na, G. Herrmann, X. Ren, M. Mahyuddin, and P. Barber, "Robust adaptive finite-time parameter estimation and control of nonlinear systems," in *Intelligent Control (ISIC), 2011 IEEE International Symposium on*, sept. 2011, pp. 1014 –1019.
[31] P. Sahlholm, *Iterative road grade estimation for heavy duty vehicle control*. Elektrotekniska system, Kungliga Tekniska hogskolan, 2008.
[32] P. Sahlholm and K. Johansson, "Road grade estimation for look-ahead vehicle control," in *Proceedings of the 17th IFAC World Congress*, 2008.
[33] S. Sastry and M. Bodson, *Adaptive control: Stability, Convergence and Robustness*. Dover Publications, 1989.
[34] N. Shimkin and A. Feuer, "Persistency of excitation in continuous system," *System and Control Letters*, pp. 225–233, 1987.
[35] J.-J. Slotine and W. Li, *Applied Nonlinear Control*. Prentice Hall, Oct. 1990. [Online]. Available: http://www.worldcat.org/isbn/0130408905
[36] T. Soderstrom and P. Stoica, *System Identification*, M. Grimble, Ed. Prentice Hall, 1989.

Muhammad Nasiruddin Mahyuddin (Corresponding author) is currently a PhD student at the department of Mechanical Engineering, University of Bristol and a member of the Nonlinear Robotics Control Group (NRCG) at the Bristol Robotics Laboratory. He received his M.Eng with high distinction in Mechatronic and Automatic Control from the Universiti Teknologi Malaysia in 2006 and obtained his B.Eng with Honours in Mechatronic Engineering from the International Islamic University of Malaysia in 2004. He was an Application Engineer at Agilent Technologies working with Motion Control products in 2004-2005. He was appointed as a Senior Associate Teacher by the University of Bristol via contract, teaching Nonlinear Control with Application to Robotics from October 2011 to July 2012. He currently holds a position as a Lecturer (in the study-leave mode) in Universiti Sains Malaysia, a top Research University in Malaysia. His current research interests include distributed adaptive control, robust nonlinear control and parameter estimation.

Jing Na received the B.S. and Ph.D. degrees from the School of Automation, Beijing Institute of Technology, Beijing, China, in 2004 and 2010, respectively. In 2008, he was a Visiting Student with the Universitat Politcnica de Catalunya, Barcelona, Spain. From 2008 to 2009, he was a Research Collaborator with the Department of Mechanical Engineering, University of Bristol, Bristol, U.K. Since 2010, he has been with the Faculty of Mechanical and Electrical Engineering, Kunming University of Science and Technology, Kunming, China. His current research interests include adaptive control, time-delay systems, neural networks, parameter estimation, repetitive control, and nonlinear control and applications. Dr. Na was a Postdoctoral Fellow with the ITER Organization, Cadarache, France, from 2011 to 2012.

Guido Herrmann received the German degree "Diplom-Ingenieur der Elektrotechnik"(with highest honours) from the Technische Universitt zu Berlin, Germany, and the Ph.D. degree from the University of Leicester, UK, in 1997 and 2001, respectively. From 2001 to 2003, he was a Senior Research Fellow at the Data Storage Institute in Singapore. From 2003 until 2005, he was a Research Associate, Fellow, and Lecturer at the University of Leicester. He joined the University of Bristol, Bristol, UK, as a Lecturer in March 2007. He was promoted in August 2009 to a Senior Lecturer and in August 2012 to the position of a Reader in Control and Dynamics. His research considers the development and application of novel, robust and nonlinear control systems. He is a Senior Member of the IEEE and a Technical Editor of the IEEE/ASME Transactions on Mechatronics and an Associate Editor of the International Journal on Social Robotics.

Xuemei Ren received the B.S. degree from Shandong University, China, in 1989, and the M.S. and Ph.D. degrees in control engineering from Beijing University of Aeronautics and Astronautics, China, in 1992 and 1995, respectively. She is currently a Professor in the School of Automation, Beijing Institute of Technology, Beijing, China. Her research interests include intelligent systems, neural networks, adaptive control and servo systems.

Phil Barber received his degree in Electrical and Control Engineering at Birmingham University. After a year at GEC's Hirst Research Centre, he joined the Automotive industry in 1985 at the Lucas Research Centre. He gained his Phd in 1992 from the University of Warwick researching fuel injected engines. Joining Jaguar in 1990, he went on to be part of the team working on steer by wire, lane keeping and adaptive cruise control (ACC) demonstrators for the PROMETHEUS project. The ACC won the Henry Ford Technical Award, the highest award for technical achievement in the Ford Motor Corporation in 2000. Then, he oversaw the changeover of military standard ACC radar manufacture to automotive production standards and he lead the ACC delivery team. He returned to Research in 2008 as the Technical Specialist for Chassis Systems and Vehicle Capability. Current interests include vehicle dynamics, state estimation, distributed and networked systems for vehicle control and regenerative braking.